AGU PUBLICATIONS

JGR

Journal of Geophysical Research: Oceans

RESEARCH ARTICLE

10.1002/2014JC010318

Mapping of sea surface nutrients in the North Pacific: Basin-wide distribution and seasonal to interannual variability

Sayaka Yasunaka[1], Yukihiro Nojiri[2], Shin-ichiro Nakaoka[2], Tsuneo Ono[3], Frank A. Whitney[4], and Maciej Telszewski[5]

[1]Center for Global Change, Japan Agency for Marine-Earth Science and Technology, Yokosuka, Japan, [2]Center for Global Environmental Research, National Institute for Environmental Studies, Tsukuba, Japan, [3]National Research Institute of Fisheries Science, Fisheries Research Agency, Yokohama, Japan, [4]Institute of Ocean Sciences, Fisheries and Oceans Canada, Sidney, British Columbia, Canada, [5]International Ocean Carbon Coordination Project, Institute of Oceanology of Polish Academy of Sciences, Sopot, Poland

Key Points:
- Monthly maps of sea surface nutrients are produced for the North Pacific
- Spatial patterns of stoichiometric ratio of seasonal drawdowns are clarified
- PDO is related to nutrient variability in the North Pacific

Correspondence to:
S. Yasunaka,
yasunaka@jamstec.go.jp

Citation:
Yasunaka, S., Y. Nojiri, S. Nakaoka, T. Ono, F. A. Whitney, and M. Telszewski (2014), Mapping of sea surface nutrients in the North Pacific: Basin-wide distribution and seasonal to interannual variability, *J. Geophys. Res. Oceans*, *119*, doi:10.1002/2014JC010318.

Received 30 JUL 2014
Accepted 19 OCT 2014
Accepted article online 24 OCT 2014

Abstract Monthly maps of sea surface nutrient (phosphate, nitrate, and silicate) concentrations were produced for the North Pacific (10°N–60°N, 120°E–90°W) for the years 2001–2010 using a selforganizing map trained with temperature, salinity, chlorophyll-a concentration, and mixed layer depth. Nutrient sampling was carried out mainly by ships of opportunity, providing good seasonal coverage of the surface ocean. Using the mapping results, we investigated the spatiotemporal variability of surface North Pacific nutrient and dissolved inorganic carbon (DIC) distributions on seasonal and interannual time scales. Nutrient and DIC concentrations were high in the subarctic in winter and low in the subtropics. In the summer, substantial amount of nutrients remained unutilized in subarctic and the northern part of the subarctic-subtropical boundary region while that was not the case in the southern part of the boundary region. In the subtropics, nutrients were almost entirely depleted throughout the year, while DIC concentrations showed a north-south gradient and significant seasonal change. Nutrients and DIC show a large seasonal drawdown in the western subarctic region, while the drawdown in the eastern subarctic region was weaker, especially for silica. The subarctic-subtropical boundary region also showed a large seasonal drawdown, which was most prominent for DIC and less obvious for nitrate and silicate. In the interannual time scale, the Pacific Decadal Oscillation was related to a seesaw pattern between the subarctic-subtropical boundary region and the Alaskan Gyre through the changes in horizontal advection, vertical mixing, and biological production.

1. Introduction

Biogeochemical cycles within the ocean are controlled to a large extent by biological processes, with nutrients playing an important role as tracers of primary production and often acting as limiting factors of the processes themselves. Surface nutrient concentrations in the global ocean show large spatial and seasonal variability which results from spatiotemporal variability of physical processes and biological activities [e.g., *Wong et al*., 2002a]. Considerable interannual variability in nutrient concentrations is also related to El Niño events and the Pacific Decadal Oscillation (PDO) in several regions of the North Pacific [e.g., *Wong et al*., 2002b; *Goes et al*., 2004; *Miller et al*., 2004].

However, nutrient observations are generally still too scarce to allow efficient basin-scale mapping, except for long-term averages such as those produced as the World Ocean Atlas (WOA) [*Garcia et al*., 2014]. Alternatively, several studies attempted to estimate surface nutrient concentration using relationship between nutrients and various seawater properties [e.g., *Chavez et al*., 1996]. *Goes et al*. [2000] showed the possibility of estimating North Pacific surface nitrate distribution using multiple linear regressions of sea surface temperature (SST) and chlorophyll-a concentration (CHL). The complex relationships between nutrient and seawater properties and domain and/or time dependence of these relationships make this approach difficult [*Garside and Garside*, 1995]. Recently, *Steinhoff et al*. [2010] successfully applied a selforganizing map (SOM) technique for estimating surface nitrate in the North Atlantic. Basin-scale estimates of partial pressure of CO_2 (pCO_2) using a SOM technique have been reported in the North Atlantic and the North Pacific, and several advantages of this mapping method were highlighted [*Lefèvre et al*., 2005; *Telszewski et al*., 2009; *Nakaoka et al*., 2013]. According to those studies, SOM can empirically induce the nonlinear relationship

Table 1. Total Number of Nutrient Observations in the North Pacific (10°N–60°N, 120°E–90°W)

	Phosphate		Nitrate		Silicate	
	All	2001–2010	All	2001–2010	All	2001–2010
NIES	7,686	6,091	8,043	6,293	7,939	6,188
IOS	13,353	5,925	13,399	5,923	13,426	5,923
PACIFICA	3,309	1,877	3,296	1,891	2,986	1,680

between parameters without any a priori assumptions of regression functions and without the need to divide the basin into subregions.

This study presents surface phosphate, nitrate, and silicate distributions in the North Pacific using a SOM trained on the SST, sea surface salinity (SSS), CHL, and mixed layer depth (MLD). The North Pacific is a large and complex basin, composed of several significantly different subregions such as the "high-nutrient and low-chlorophyll" (HNLC) subarctic region [*Martin et al*., 1994] or the oligotrophic subtropical region [*Morel et al*., 2010]. In addition, a strong east-west contrast of seasonal nutrient variability in the subarctic exists [*Wong et al*., 2002a; *Harrison et al*., 2004]. Therefore, the SOM technique seems to be better suited for the task than more traditional statistical techniques based on linear regressions. In the present study, we created 120 monthly sea surface nutrient (phosphate, nitrate, and silicate) concentration maps from January 2001 to December 2010 for the North Pacific (10°N–60°N, 120°E–90°W). Using the mapping results, we investigated spatiotemporal variability of the North Pacific nutrient concentration on seasonal and interannual time scales.

2. Data

2.1. Discrete Water Samples for Nutrients

For nutrient mapping, we used surface measurements of phosphate, nitrate (nitrate plus nitrite, hereafter referred as nitrate), and silicate concentrations conducted by National Institute for Environmental Studies (NIES, Japan) and Institute of Ocean Science (IOS, Canada). We also included nutrient observations archived in the Pacific Ocean interior carbon (PACIFICA) database.

NIES has carried out ship of opportunity sampling on the MS Skaugran (1995–1999), MS Alligator Hope (1999–2001), and MS Pyxis (2002–2013) between Japan and North America, and the MS Trans Future 5 (2006–present) between Japan and Oceania. Surface samples (5–10 m depth) were manually collected from the seawater lines installed for pCO_2 observation intakes [*Murphy et al*., 2001], routinely at 2 or 3 samples per day (at about 200–400 km intervals). Sampled nutrient tubes were stored frozen and then analyzed by colorimetric techniques in the NIES laboratory. The number of surface nutrient samples analyzed by NIES in the North Pacific amounts to about 7900 in total, of which 6100 were taken during the study period (Table 1), with measurements well distributed throughout the study area (Figure 1a). IOS also carried out ship of opportunity surface sampling (5–10 m depth) between Japan and North America from 1987 to 2010 [*Whitney*, 2011], collecting approximately 6000 samples from 2001 to 2010 (Table 1) mainly in the subarctic region (Figure 1b). The PACIFICA database contains hydrographic/hydrochemical data from research cruises (http://cc-s.pices.jp/) [*Suzuki et al*., 2013]. We extracted the shallowest values from the upper 20 m in each cast. PACIFICA archived approximately 1800 nutrient samples over the 2001–2010 period (Table 1 and Figure 1c). We confirmed any significant and systematic biases were not apparent among these three data sets. As a whole, temporal and spatial coverage of observational data did not prominently fluctuate throughout the study period within the study region (not shown here).

We used the surface (standard depth of 10 m) nutrient samples archived in World Ocean Database 2013 (WOD13) [*Boyer et al*., 2013] as completely independent data for validation of mapping results. Nutrient samples total to approximately 4000 in the North Pacific from 2001 to 2010, although most of the data were collected outside of the central part of the basin (Figure 1d). Duplicates with data archived in PACIFICA were excluded from the validation process, while NIES and IOS observations have not been included in WOD13.

2.2. Other Gridded Data Sets

We used four physical and biogeochemical data sets, SST, SSS, MLD, and CHL to train the SOM. SST and SSS are indicators of water type (subarctic, subtropical, upwelled, etc.), MLD represents vertical entrainment of nutrients, and CHL approximates the biological nutrient consumption.

SST data were obtained from the National Oceanic and Atmospheric Administration (NOAA) optimum interpolation SST version 2 with a 1° × 1° monthly resolution (http://www.esrl.noaa.gov/psd/data/gridded/data.

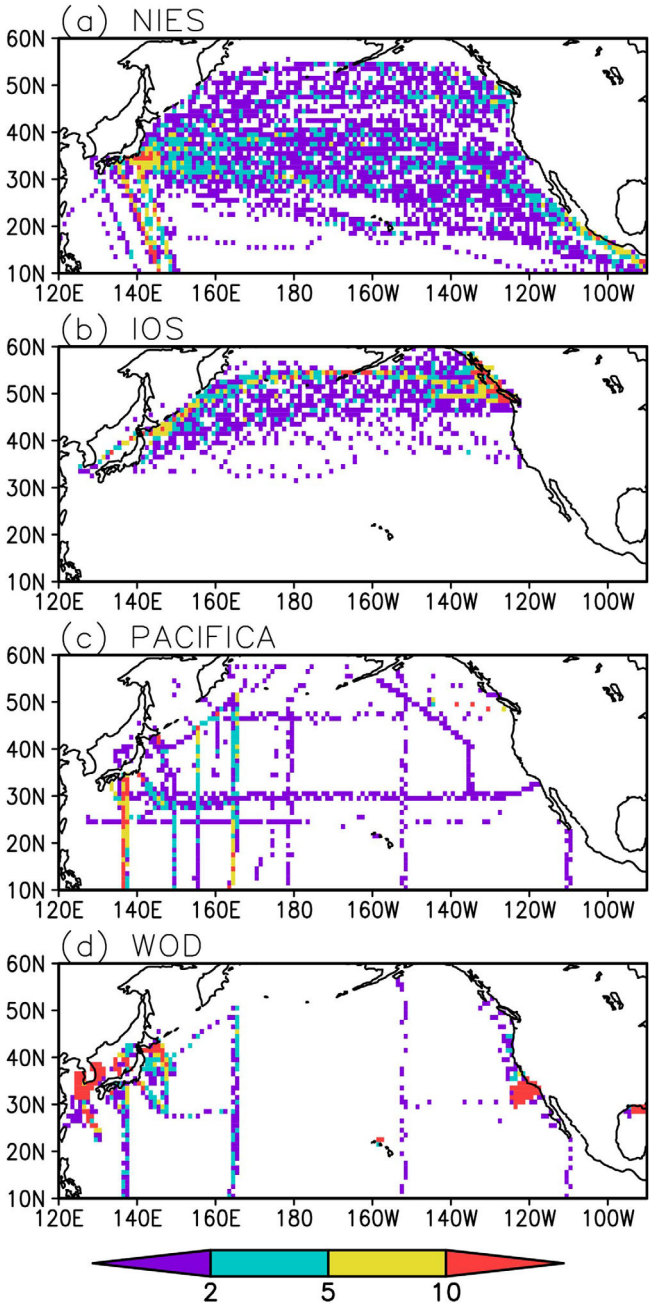

Figure 1. Number of nitrate observations from 2001 to 2010 archived in (a) NIES, (b) IOS, (c) PACIFICA, and (d) WOD13.

noaa.oisst.v2.html) [*Reynolds et al.*, 2002]. SSS data come from the Japan Agency for Marine-Earth Science and Technology (JAMSTEC) objective analysis at 1° × 1° monthly resolution (MOAA_GPV; http://www.jamstec.go.jp/ARGO/argo_web/MapQ/Mapdataset.html) [*Hosoda et al.*, 2008].

MLD data used are the monthly climatology produced by JAMSTEC (MILA_GPV; http://www.jamstec.go.jp/ARGO/argo_web/MILAGPV/index_e.html) [*Hosoda et al.*, 2010]. Although MLD would vary interannually, it is closely related with interannual variability in SST [*Carton et al.*, 2008]. Missing MLD at individual grid pints were filled by interpolating values from surrounding grid points for which data exist.

Monthly CHL data were obtained from SeaWiFS Level 3 standard products provided by National Aeronautics and Space Administration (NASA; http://oceancolor.gsfc.nasa.gov). We rescaled the CHL data into the 1° × 1° grids from the original resolution of 9 km. CHL data sets included many grids with missing values caused by cloud cover and the acute angle of the sun (about 5% in the subtropics and 20% in the subarctic have missing values in both data sets). To improve the data coverage, we combined the SeaWiFS CHL with the MODIS-Aqua CHL, which are provided by NASA since July 2002. Although significant biases between the data sets have been pointed out [*Morel et al.*, 2007], we found that anomalies from respective 8 year monthly mean from 2003 to 2010 were correlated with each other, and differences were less than 20% of the absolute values in most of the analysis domain (not shown here). Therefore, we filled the grids with missing values in SeaWiFS CHL with bias-adjusted MODIS-Aqua CHL (i.e., 8 year monthly mean SeaWiFS CHL plus MODIS-Aqua CHL anomaly subtracting from 8 year monthly mean MODIS-Aqua CHL). This procedure reduced the percentage of empty grids from 10% to 3%. The remaining empty grid points were filled by interpolating values from surrounding nonempty grids. As a result, we obtained complete CHL maps in the North Pacific, except for high latitude area (north of 45°N) from November to January due to the low angle of the sun.

Ocean surface dissolved inorganic carbon (DIC) concentrations from 2002 to 2008 were produced by *Yasunaka et al.* [2013] from pCO_2 produced using a SOM technique by *Nakaoka et al.* [2013] and total alkalinity

calculated using the simple empirical function of *Lee et al*. [2006] (http://soop.jp/index.html). We also used monthly air-sea CO_2 flux calculated in *Yasunaka et al*. [2013] from ocean surface pCO_2 [*Nakaoka et al*., 2013] by using the gas exchange coefficient of *Sweeney et al*. [2007].

Surface current velocity data come from monthly means satellite-derived Ocean Surface Current Analysis (OSCAR; http://www.oscar.noaa.gov/) [*Bonjean and Lagerloef*, 2002]. Monthly fields of net primary production (NPP) were obtained from the Ocean Productivity website (http://www.science.oregonstate.edu/ocean.productivity/index.php) with a spatial resolution of 1/6° × 1/6°, which were calculated by using the vertically generalized production model (VGPM) of *Behrenfeld and Falkowski* [1997].

3. Nutrient Mapping

Nutrient concentrations were mapped for 120 months from January 2001 to December 2010 over the area of the North Pacific (10°N–60°N, 120°E–90°W) and southern Bering Sea (south of 55°N). We excluded the northern part of the Bering Sea, Okhotsk Sea, and Japan Sea which had limited in situ nutrient observations (Figure 1). Coastal areas (bathymetric depth <200 m) were also excluded since the relationships between nutrients and physical/biogeochemical properties are significantly different due to the influences of tidal mixing, estuarine circulation, and riverine discharge [*Whitney et al*., 2005].

3.1. Gridding Procedure of Nutrient Discrete Samples

First, we gridded discrete nutrient samples from NIES, IOS, and PACIFICA into 1° × 1° monthly boxes from 2001 to 2010 for mapping.

In order to eliminate extreme and/or erroneous data, we calculated long-term means (i.e., climatology) and standard deviations in 1° × 1° monthly grid boxes with the average window size of ±2 in month, ±10° in latitude, and ±30° in longitude from all of NIES, IOS, and PACIFICA surface nutrient data. We then eliminated the data whose difference from the climatology exceeded three standard deviations of the climatology. Next we recalculated the climatology and associated standard deviation using a smaller window size and eliminated extreme data again. This procedure was iterated three times while gradually reducing the window size; their sizes in month, in latitude, and in longitude were (±2, ±5°, ±10°), (±1, ±5°, ±10°), and (±1, ±2°, ±5°), respectively. As a result, we excluded about 300 measurements as extreme and/or erroneous data from 2001 to 2010 for phosphate, nitrate, and silicate, respectively. Finally, we averaged the remaining observations onto 1° × 1° monthly grid boxes of each year from 2001 to 2010.

The discrete nutrient samplings from the WOD13 were also gridded into 1° × 1° monthly boxes from 2001 to 2010 for validation of mapping results. We only used data with a quality control flag of 0 (i.e., accepted value).

3.2. Nutrient Estimation Using Selforganizing Map

Our method for estimating nutrient concentrations is similar to that of *Telszewski et al*. [2009] and *Nakaoka et al*. [2013] except that several settings were altered for appropriate estimation of the nutrient concentration in the North Pacific. The main difference was the addition of latitude (LAT) and longitude (LON) to the set of training parameters in order to avoid systematic spatial bias.

Three steps were taken to estimate basin-wide nutrient fields: first, dividing the 1° × 1° monthly North Pacific grids into 5000 groups using a SOM of SST, SSS, CHL, MLD, LAT, and LON; second, labeling the preconditioned SOM with the observed nutrient concentrations based on corresponding SST, SSS, CHL, and MLD values; third assigning nutrient concentrations to all grids using the labeled SOM and mapping the estimated distribution onto the North Pacific according to their time and space coordinates. Labeling and assigning were done for phosphate, nitrate, and silicate separately. We used the SOM Toolbox Version 2, developed by the Laboratory of Information and Computer Science at the Helsinki University of Technology (http://www.cis.hut.fi/projects/somtoolbox) for creating the SOM.

The CHL data were affected by the lack of satellite coverage from November to January at high latitude (north of 45°N) as mentioned above. In order to make up for the blank area of CHL in these months, we computed the second set of estimates using the SOM trained with five parameters SST, SSS, MLD, LAT, and LON. We then generated complete nutrient maps in the study area by combining the estimated nutrient values obtained with the six parameter SOM including CHL with the values obtained with the five parameter SOM. We checked the difference between the nutrient values estimated with the six-parameter SOM

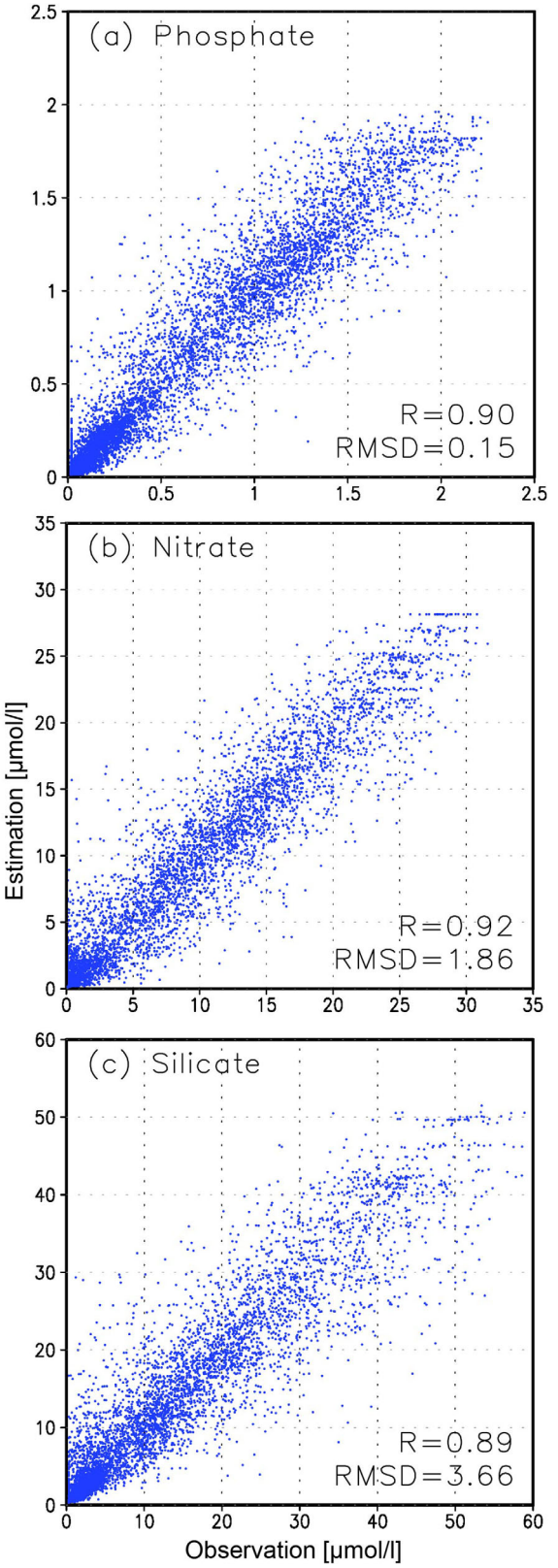

Figure 2. Relationship between measured and estimated nutrient concentrations. (a) Phosphate, (b) nitrate, and (c) silicate.

and the five-parameter SOM in the region between 40°N and 45°N and found the difference to be comparable to the uncertainty of the estimation (see section 3.3) from November to January. This most likely results from relatively low biological activity during the winter at high latitudes [e.g., *Imai et al.*, 2002].

From these procedures, we obtained 120 monthly basin-wide nutrient maps from January 2001 to December 2010.

3.3. Uncertainty

For the whole North Pacific, correlation coefficients between the estimated values and in situ observations gridded into 1° × 1° monthly boxes were within 0.89−0.92, and root-mean-square difference (RMSD) were 0.15 μmol/L for phosphate, 1.86 μmol/L for nitrate, and 3.66 μmol/L for silicate (Figure 2). Scatterplots of the estimated and observed nutrients show that the values are clustered around the 1:1 line. The differences between the estimated values and observations came from not only estimated error but also error in gridded samples. The number of observations in 1° × 1° monthly grid box of each year was almost one, that is, sampling error would be as large as the nutrient variation in 1° × 1° monthly grid box. Incidentally, standard deviations of nutrient monthly climatology in 1° × 1° grid were about 90% of RMSD between the SOM estimates and the observed values.

We also compared our estimates with observations in box-averaged time series, finding two areas where sufficient WOD13 data existed (Figure 3). Box-mean time series of estimated nutrient concentrations were in good agreement with observations (not only data used for mapping but also independent data of WOD13; Figure 3). Our estimates represented large seasonal variability with summer depletion except for several extreme values in East Japan area (36°N–40°N, 140°E–150°E), as well as constant concentrations at different values between respective nutrients along the California coast (30°N–35°N, 130°W–115°W). Interannual variability of the SOM estimates and observations also appeared to be in phase. For example, nutrient concentrations in 2001–2002 and 2007–2009 winters were lower than those in 2003–2006 winters in East Japan region.

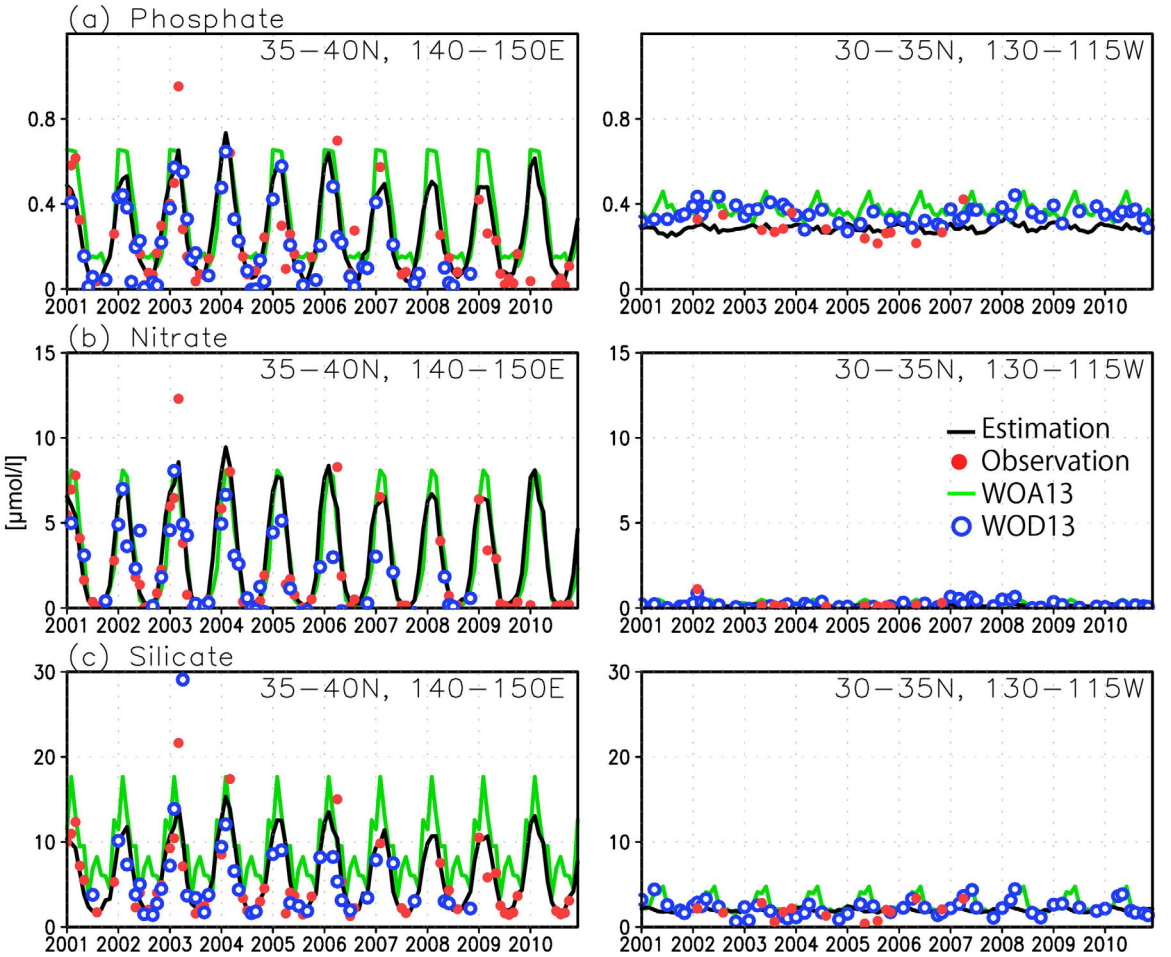

Figure 3. Area-mean time series of estimated (black line) (a) phosphate, (b) nitrate, and (c) silicate concentrations with observations (red circle, labeling data; blue circle, independent data; (left) 35°N–40°N, 140°E–150°E; (right) 30°N–35°N, 130°W–115°W).

We examined the differences between the monthly climatology obtained from our study and WOA 2013 (WOA13) climatology (see Appendix A). We confirmed that our maps not only reproduced basin-scale features of nutrient distributions which appear in WOA13 with finer spatiotemporal resolution than WOA13, but also retained consistency in time and among the nutrient components which allow us to investigate spatiotemporal variability.

4. Seasonal Variability

We explored seasonal patterns using 10 year monthly mean nutrient concentrations. In this section, we also examined seasonal variability of the sea surface DIC concentration estimated by *Yasunaka et al.* [2013]. We calculated the 7 year monthly mean DIC concentration to match the temporal extent of the DIC estimates that spun out from 2002 to 2008.

4.1. Clustering Method

We used cluster analysis to divide the North Pacific into nine areas with similar nutrient and DIC long-term monthly mean concentrations. Here we used *k*-means clustering, which aims to partition observations into certain number of clusters in which each observation belongs to the cluster with the nearest mean. In order to eliminate initial value dependence, we repeated the clustering 1000 times and used the minimum solution with the within-cluster sums of point-to-centroid distances. Before the clustering, we normalized nutrient and DIC climatologies by the annual means of the monthly climatology averaged over the North Pacific and their seasonal amplitudes. As a result, the subarctic was divided into four clusters in the northwest-

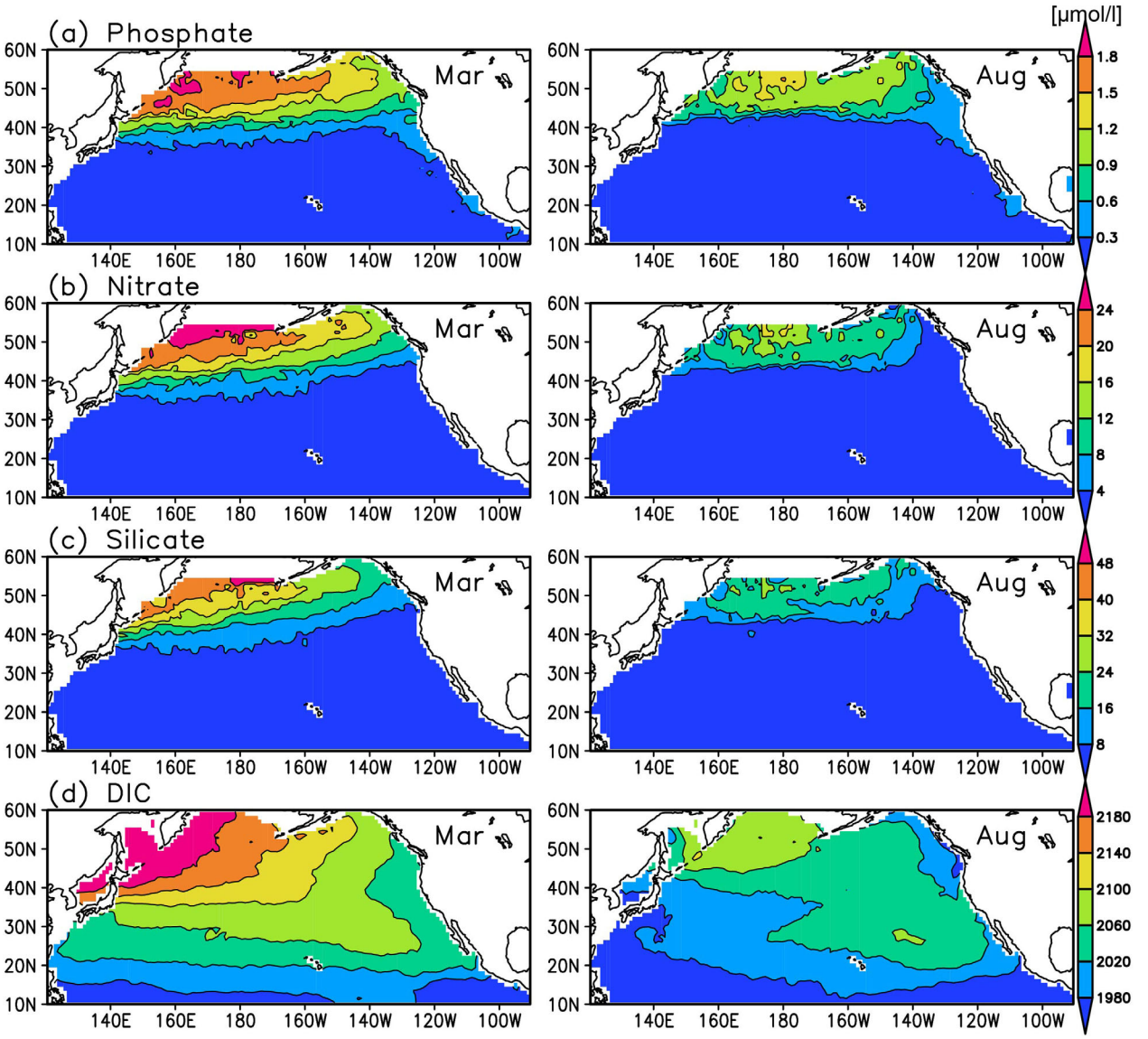

Figure 4. Long-term monthly means for (a) phosphate, (b) nitrate, (c) silicate, and (d) DIC concentrations in (left) March and (right) August.

southeast direction, the subarctic-subtropical boundary region into two in the north-south direction, and the subtropics into three in the north-south direction (Figure 5a). Nine was the minimum number of clusters that represented the difference between the western midlatitudes and the eastern subarctic.

4.2. Spatiotemporal Distribution

Spatial distributions of long-term monthly mean concentration are shown for March and August in Figure 4, and cluster-mean monthly climatologies are summarized in Figures 5b–5e.

Nutrient and DIC concentrations were high in the subarctic (Areas A, B, C, and D) and low in the subtropics (Areas G, H, and I) throughout the year. They reached maximum concentrations in March, and minimum concentrations in August or September in all areas.

The north-south gradient from subarctic to the subarctic-subtropical boundary region was steeper for the three nutrients than for DIC, especially in winter, mainly because the salinity effect on DIC reduced the DIC north-south contrast as discussed in *Yasunaka et al.* [2013].

In the summer, substantial amounts of nutrient remained only in subarctic North Pacific region (Areas A, B, C, and D), and the northern part of the subarctic-subtropical boundary region (Area E). The division line

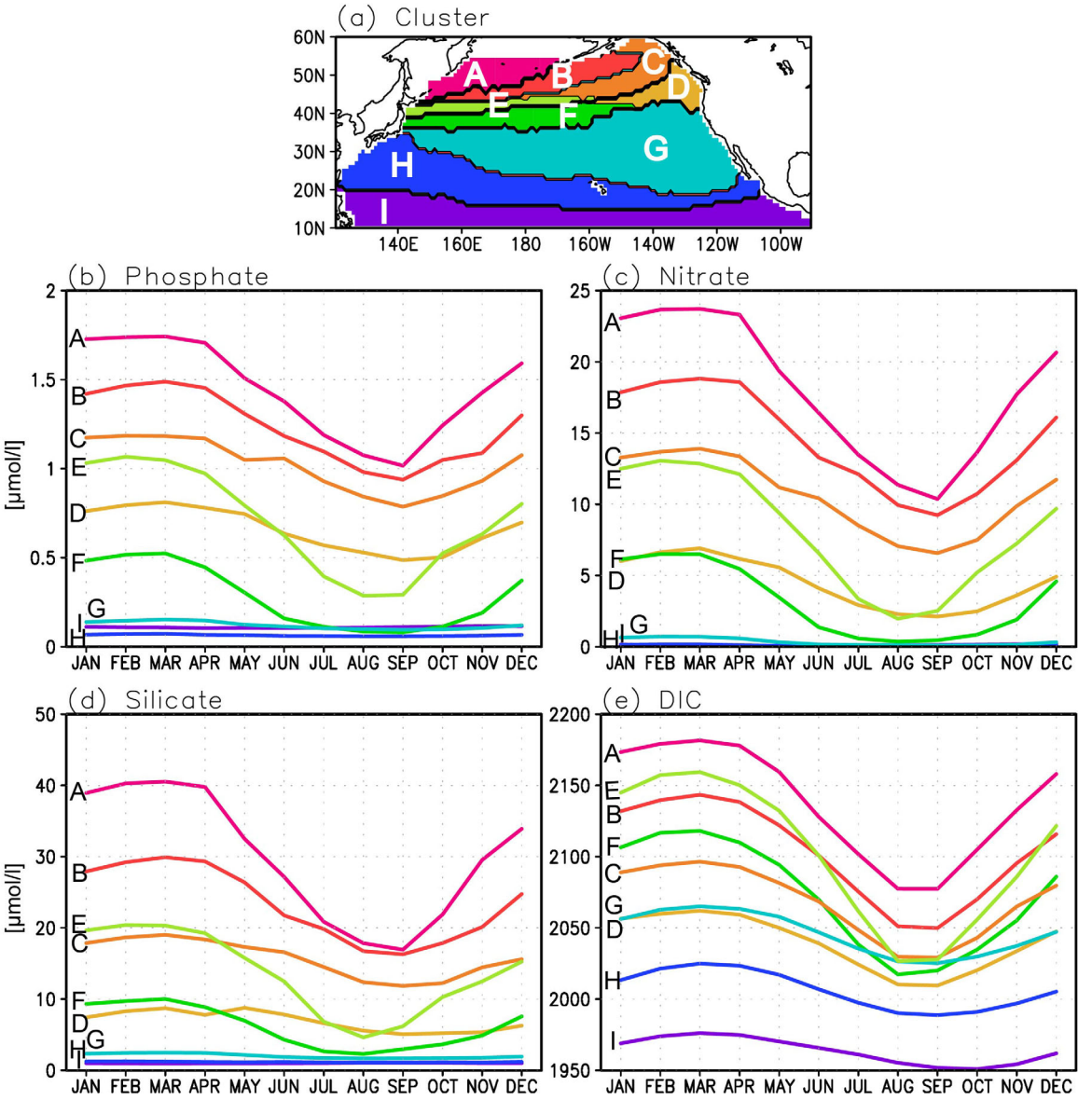

Figure 5. Spatial distribution of nine areal clusters for (a) monthly climatologies of nutrient and DIC concentrations and (b) monthly climatologies averaged in each cluster for phosphate, (c) nitrate, (d) silicate and (e) DIC. In Figures 5b–5d, seasonal variation in each cluster is drawn by the same color as shown in (a) cluster map.

across around 40°N suggests that the limiting factors governing biological production differs between the northern half (probably light and/or iron, the HNLC domain) and the southern half (nutrients) of the subarctic-subtropical boundary region. Although the boundary between limiting factor has been roughly described [e.g., *Polovina et al*., 1995], the switch between limiting factor results in different responses to climate variability across about 40°N as described in section 5.

Both monthly mean and seasonal concentration decrease from winter to summer are larger in the western subarctic (Area A) than in the east (Areas B, C, and D). A difference of seasonal nutrient decrease between Areas A and B is mainly due to the difference of winter concentration; summer concentrations show almost no difference between these two areas, especially in the case of silicate. *Nishioka et al*. [2007, 2011] showed that main source of iron to the surface waters of western subarctic North Pacific region is winter mixing rather than airborne dust input. If we assume that iron supply in central subarctic North Pacific region also results from winter mixing, we can expect that iron concentration in winter waters of Areas A and B differ similarly to nutrient and that nutrient drawdown in both areas stops with same nutrient concentration level corresponding to iron depletion.

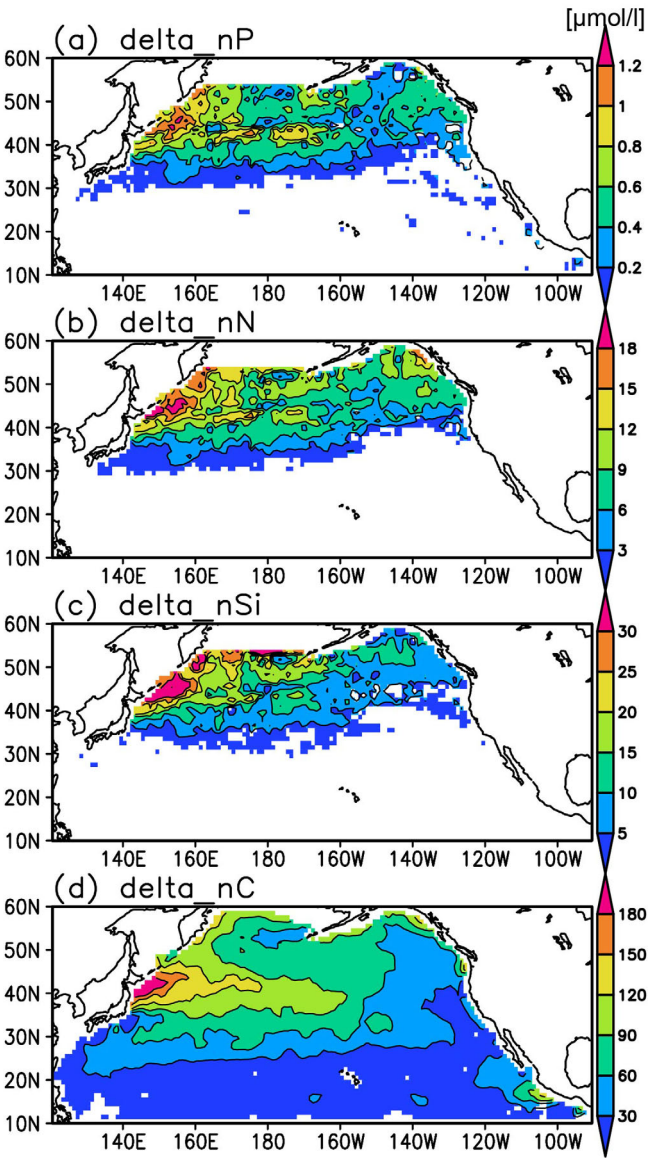

Figure 6. Seasonal drawdown (March minus August) of salinity-normalized (a) phosphate, (b) nitrate, (c) silicate, and (d) DIC. Effect of horizontal advection and effect of air-sea CO_2 flux were eliminated. Only drawdowns larger than error variance of mapping uncertainty (e.g., sqrt(2 × (0.15^2/10)) for phosphate) are colored.

In the subtropics, nutrients are generally depleted throughout the year (Areas G, H, and I). On the other hand, DIC concentrations showed north-south contrast and seasonal decrease throughout the subtropics.

4.3. Seasonal Drawdown

We explored the seasonal drawdown of nutrients and DIC in more detail. Nutrient and DIC concentrations decrease mainly due to biological consumption when the mixed layer shoals from winter to summer and increase by entrainment of nutrient and DIC-rich water when the mixed layer deepens from summer to winter [*Takahashi et al.*, 1993]. Here we examined nutrient and DIC changes between late winter (March) maxima and summer (August) minima.

Beyond biological consumption, other processes affecting the seasonal drawdown of nutrients include horizontal advection, dilution/condensation, air-sea flux, and vertical diffusion. We calculated $\mathbf{u}\cdot\nabla N$ ($\mathbf{u}$ is the horizontal velocity, N is the nutrient or DIC concentration) as the horizontal advection effect. This estimate shows that advection accounts for less than 10% of the seasonal drawdown. In order to eliminate the dilution/condensation effect due to precipitation/evaporation, we used salinity-normalized nutrient and DIC concentrations (to S = 35). Salinity effect was negligibly small except in the equatorial upwelling region for DIC. We also took account of the effects of air-sea CO_2 flux, due to differences between ocean and atmosphere pCO_2, on the DIC change. We estimated the surface DIC change from month m1 to month m2 due to CO_2 flux using the formulation of *Lee* [2001]:

$$(\mathrm{DIC_{m1}}-\mathrm{DIC_{m2}})_{\mathrm{flux}}=\sum_{m=m1}^{m2-1}\left[(\mathrm{FLUX_m}/\mathrm{MLD_m})+(\mathrm{FLUX_{m+1}}/\mathrm{MLD_{m+1}})\right]/2, \quad (1)$$

where subscript denotes month and FLUX represents air-sea CO_2 flux (plus indicates efflux and minus influx), under the assumption that biogeochemical parameters are constant in the mixed layer. The North Pacific absorbs more than 20 μmol/L CO_2 from the atmosphere, especially in the subtropical/subarctic boundary region and along the western coast of the North America from March to August. Atmospheric input of nutrients was not assessed, since its contribution was estimated to be smaller than 10% in the open ocean [*Krishnamurthy et al.*, 2010]. We also assumed that vertical diffusion was negligible during the mixed layer shoaling period [*Lee*, 2001]. We calculated seasonal drawdown from concentration changes,

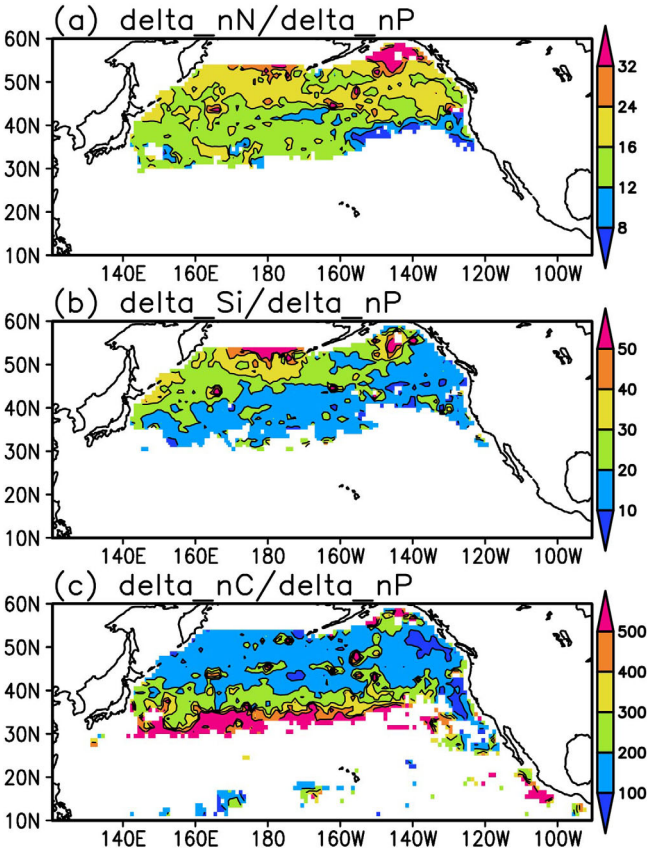

Figure 7. Stoichiometric ratios of seasonal salinity-normalized nutrient and DIC decreases from March to August; (a) ΔnN/ΔnP, (b) ΔnSi/ΔnP, (c) ΔnC/ΔnP. Effect of air-sea CO_2 flux on the DIC change was also taken account. Only ratios larger than error variance of mapping uncertainty are colored.

subtracting the effects of horizontal advection, dilution/condensation, and air-sea flux. The resultant seasonal drawdown is shown in Figure 6, accompanied by maps of drawdown ratio among nutrients and DIC in Figure 7.

All three nutrients show prominently large seasonal drawdown in the western subarctic (Area A), confirming the status of this region as one of the highest biological production areas in the world oceans [*Honda et al.*, 2002]. Seasonal drawdown in the central and eastern subarctic region (Areas B, C, and D) decreased eastward toward the North American coast, as described in section 4.1. The eastward weakening of drawdown in the subarctic was most prominent for silicate.

Large seasonal drawdowns were also found in the northwestern area of the subarctic-subtropical boundary region (Area E), that is, seasonal drawdowns did not monotonically increase from south to north but showed double peaks in a north-south direction. In this area, nutrient-rich waters are transported southward from the Bering Sea by the Oyashio Current and are enriched with iron from the Sea of Okhotsk [*Whitney*, 2011; *Nishioka et al.*, 2011]. The local maximum in the subarctic-subtropical boundary region was most prominent for DIC and less obvious for nitrate and silicate.

The drawdown ratio of nitrate and phosphate (ΔnN/ΔnP) was near the Redfield stoichiometry (ca. 16) in a wide area north of 40°N, while it drops below 16 south of this latitude (Figure 7a). This is attributed to nitrogen fixation, which is thought to occur mainly in the tropical and subtropical North Pacific by a numerical model [*Deutsch et al.*, 2007] and by direct observations [*Shiozaki et al.*, 2010]. Our results indicate that the distribution of N_2-fixation-affected waters can be determined based on surface nutrient utilization. Moreover, N_2-supported production would be calculated by methodology similar to that suggested by *Lee et al.* [2002].

Drawdown ratio of silicate and phosphate (ΔnSi/ΔnP) shows north-south contrast and subarctic east-west contrast (Figure 7b). The difference in ΔnSi/ΔnP between the subarctic and subtropical/subarctic boundary regions reflects the fact that silicate-independent phytoplankton is responsible for much of the summer production in this area [e.g., *Saito et al.*, 2002]. The difference in east and west subarctic ΔnSi/ΔnP suggests that diatom production is more dominant toward the Asian coast. A clear spring increase in diatoms was observed, and coccolithophore abundance was low at/near station KNOT (44°N, 155°E), while coccolithophores and other small phytoplankton were abundant especially in late spring, and diatom comprised a minor component at station P (50°N, 145°W) [*Harrison et al.*, 2004, and their references]. Silicate inputs from rivers [*Whitney et al.*, 2005] would also be related to small ΔnSi in the eastern subarctic.

Since the north-south gradient was larger in DIC than other nutrients, ΔnC/ΔnP increased southward (Figure 7c). Value of ΔnC/ΔnP in the subarctic North Pacific was around 100–150, which is expected for ecosystems following normal Redfield stoichiometry. In the waters south of 40°N, ΔnC/ΔnP reaches values higher

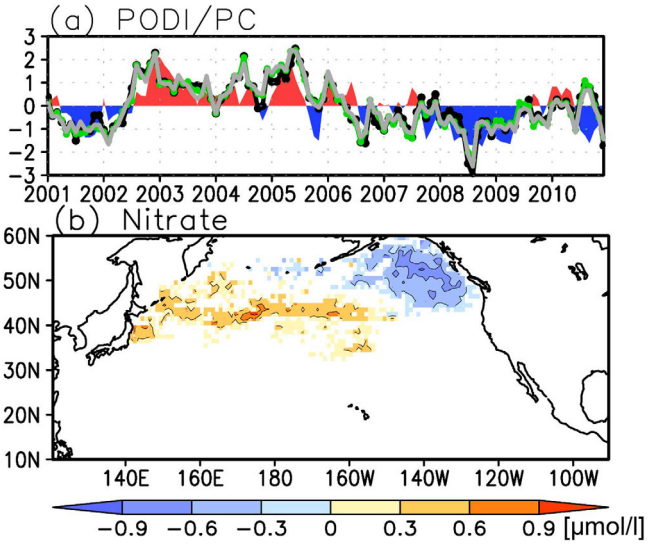

Figure 8. (a) PDO index (red and blue shadings) and PC1s for monthly nutrient anomaly (black line: phosphate, green line: nitrate, gray line: silicate). (b) Nitrate regression patterns with the PDO index. Only regression coefficients larger than error variance of mapping uncertainty (i.e., sqrt(1.86^2/120)) are colored.

than 200. *Hashihama et al.* [2013] recently found that microbes in the subtropical North Pacific can use labile dissolved organic phosphorus (LDOP) as well as inorganic phosphate. Extremely high $\Delta nC/\Delta nP$ values over 200 could be achieved when the LDOP decomposition processes occur.

5. Interannual Variability

In order to assess interannual variability, we calculated nutrient anomalies from our 10 year monthly climatologies. Then we applied EOF analysis in the nutrient anomaly fields and obtained the dominant variability modes. The first modes of all three nutrients fluctuated in low frequency, with a positive tendency from mid-2002 to mid-2006 and negative tendency before mid-2002 and in 2008 to 2009 (Figure 8a; explained variances were about 20% of total variance longer than 1 year). Spatial patterns of three nutrients were quite similar to each other (differences were below the error variance) and showed positive sign in the boundary region between subtropics and subarctic and in the western subarctic and negative sign in the Alaskan gyre (nitrate shown as an example in Figure 8b). In the subarctic-subtropical boundary region and in the western subarctic, nutrient concentrations were relatively high compared with the normal states from mid-2002 to mid-2006, and low before mid-2002 and in 2008–2009. Nutrient concentrations in the Alaskan Gyre varied in an opposite manner.

Figure 9a shows the mean nitrate concentration in 2003–2004 and 2008 when the time series of the first EOF mode were positive and negative all year, respectively. Compared with 2008, the 2003–2004 contours in the Alaskan Gyre shifted north or westward, although a position change in the central Pacific was not clear. Nitrate difference between 2003–2004 and 2008 was positive in the subarctic-subtropical boundary region and in the western subarctic and negative in the eastern region (Figure 9b), which was quite similar with the spatial pattern of the first EOF mode (Figure 8b). Changes were small south of 35°N. Phosphate and silicate concentrations also changed in the same way (not shown here). As a result, the seesaw pattern between the subarctic-subtropical boundary region and the Alaskan Gyre was the dominant feature of the nutrient variability.

The PDO is a dominant pattern of low-frequency climate variability in the North Pacific [*Mantua et al.*, 1997]. The time coefficient of the nutrient first EOF modes correlated well with the PDO index (http://jisao.washington.edu/pdo/PDO.latest; correlation coefficients were 0.60 for phosphate, 0.63 for nitrate, and 0.59 for silicate; statistically significant at the 1% level; Figure 8a). SST regression maps against the time coefficients of the nutrient first modes showed the typical PDO-related pattern with negative anomaly in the western and central North Pacific surrounded by positive anomaly (not shown here). Observed nutrient concentrations also negatively correlated with the PDO index in Areas C and D of the eastern subarctic (statistically significant at the 1% level), as *Peña and Varela* [2007] showed along Line P. Generally speaking, a 10 year period analyzed in this study does not entitle the authors to conclude on characterization of PDO variability. However, the PDO showed significant phase shifts during the study period, which is reflected in the PDO being detected as the dominant mode suggesting that PDO indeed controls the nutrient variability in the region. This result will have to be revisited once observational data for another decade will become available allowing for analysis on decadal time scales.

Next, we examined how the PDO associated with nutrient variability in the North Pacific through interannual changes in horizontal advection, vertical mixing, and biological consumption. We investigated the effect of horizontal advection by the anomalous flow across the mean nutrient gradients ($\mathbf{u}' \cdot \nabla \overline{N}$, where the

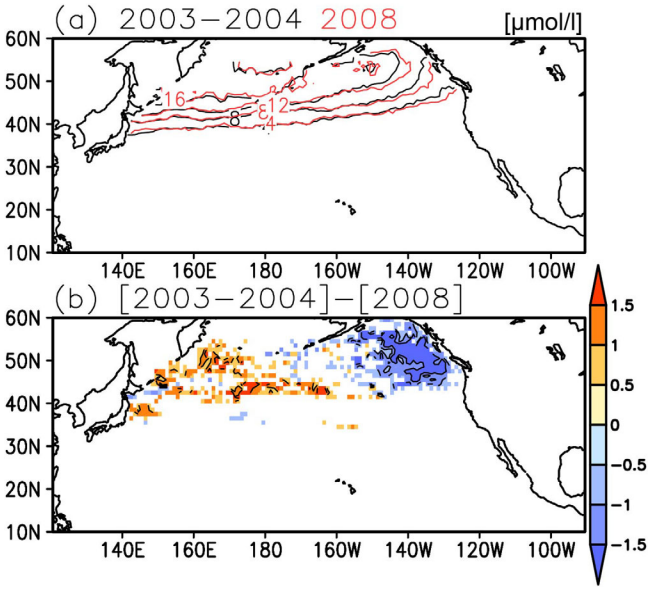

Figure 9. Nitrate concentration in (a) 2003–2004 (black) and 2008 (red), and (b) their difference. Only differences larger than error variance of mapping uncertainty (i.e., sqrt((1.86^2/24) + (1.86^2/12))) are colored in Figure 9b.

prime represents anomaly, and the overbar represents the 7 year mean), because the mean flow across the anomalous nutrient gradient ($\overline{\mathbf{u}}\cdot\nabla N'$) was small (not shown here). We used SST, in place of MLD that is related to vertical entrainment, since interannual variability in MLD is closely related to that of SST [*Carton et al.*, 2008]. Changes in NPP serve as a measure of biological production of biomass exportable to higher trophic levels or to the deep ocean as detritus [*Eppley and Peterson*, 1979].

Figure 10 shows the regression patterns of SST, horizontal advection, and NPP onto the PDO index. Nutrient change associated with the PDO was generally the opposite sign with SST and the same with the horizontal advection patterns throughout the North Pacific. However, NPP patterns showed the same polarity south of 40°N, but the opposite in the subarctic.

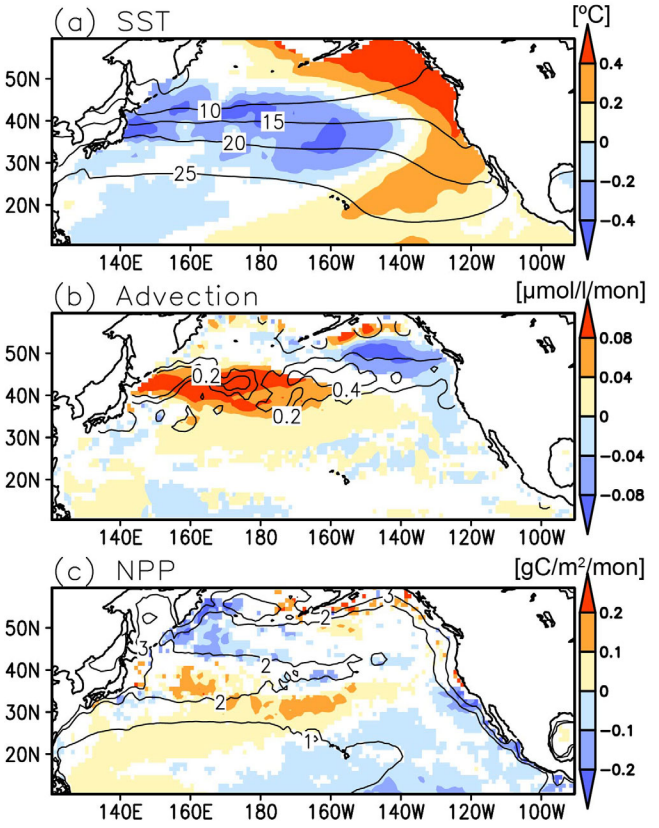

Figure 10. (a) SST, (b) nitrate horizontal advection, and (c) NPP regression patterns onto the PDO index. Only regression coefficients with correlation of $p < 0.1$ are colored. Contours indicate the 10 year mean state in each field.

The nutrient changes are interpreted in relation to the physical and biogeochemical field change associated with the PDO. When the PDO was in the positive phase, SST was cool and MLD was deep in the western Pacific due to the intense dry cold wind from the Asian Continent [*Cayan*, 1992; *Miller et al.*, 1994]. At the same time, SST was warm and MLD was shallow in the eastern Pacific due to a southerly wind anomaly and downwelling coastal Kelvin wave from the equatorial ocean [*Cayan*, 1992; *Millar et al.*, 1994; *Zhang et al.*, 1997]. An MLD deepening (shoaling) would induce a nutrient increase (decrease) via enhancement (weakening) entrainment of the subsurface nutrient-rich water, as shown by *Signorini et al.* [2001] at Station Papa (50°N, 145°W).

Changes of winds associated with the PDO [e.g., *Mantua et al.*, 1997] induced changes in horizontal advection (Ekman transport) in the midlatitudes. When the PDO was in positive phase, stronger westerly

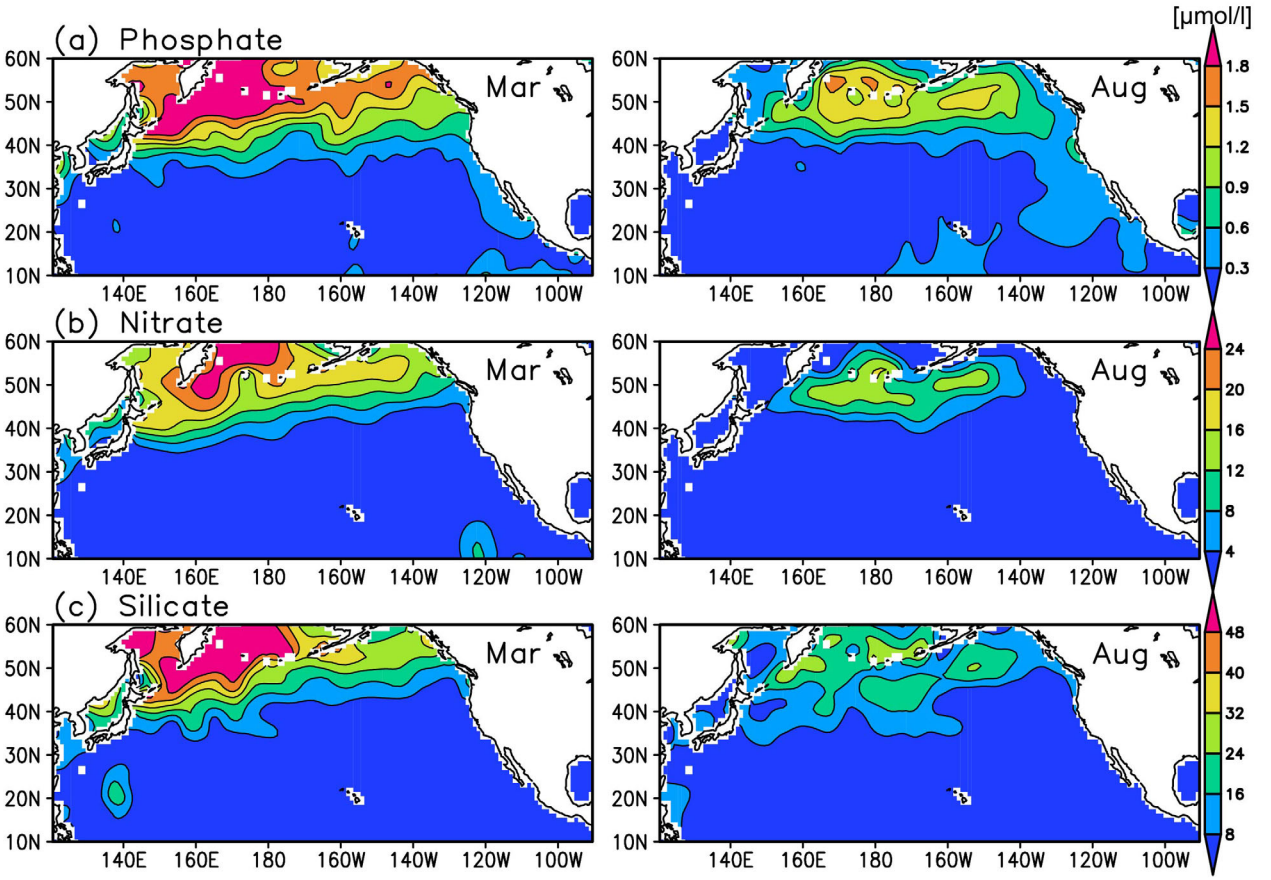

Figure A1. WOA13 climatology of (a) phosphate, (b) nitrate, and (c) silicate concentrations in (left) March and (right) August.

winds force high nutrient water southward from the subarctic to the midlatitudes, and southeasterly wind anomaly brings low-nutrient water northeastward in the eastern subarctic. Horizontal advections for phosphate and silicate were similar to that of nitrate (not shown here).

NPP anomaly north of 40°N showed the same polarity with SST but the opposite in the subtropics, which indicated that NPP anomaly north of 40°N showed opposite polarity with the MLD but was the same in the subtropics. This relationship is consistent with the simple conceptual theory espoused by *Polovina et al*. [1995]. As MLD deepens in the subtropics, where a limiting growth factor is nutrients, the entrainment of nutrient-rich water stimulates NPP. MLD shoaling in the subarctic, where a limiting factor is light, confines phytoplankton in the euphotic zone, increases NPP, and decreases nutrient levels.

The PDO-related nutrient variation pattern obtained by this study was similar to but slightly different from the PDO-related DIC variation pattern reported by *Yasunaka et al*. [2014]. In the subtropics, there was a significant DIC signal, but no nutrient signal due to differences in response to salinity change (strong in DIC while weak in nutrients). The positive nutrient signal stretched much more prominently east to west along the subarctic-subtropical boundary than that of DIC, since the north-south gradient of the concentrations was steeper in nutrient than in DIC.

6. Summary

This study produced 120 monthly maps of sea surface nutrient (phosphate, nitrate, and silicate) concentrations for the North Pacific for years 2001–2010 using a SOM trained with the SST, SSS, CHL, and MLD. We explored spatial distributions of nutrient seasonal drawdowns and their stoichiometric ratios. We also elucidated patterns of basin-wide interannual nutrient variability associated with the PDO. Surface nutrient samplings by NIES and the monthly nutrient concentrations presented in this paper are available at the NIES-hosted web page (http://soop.jp/index.html).

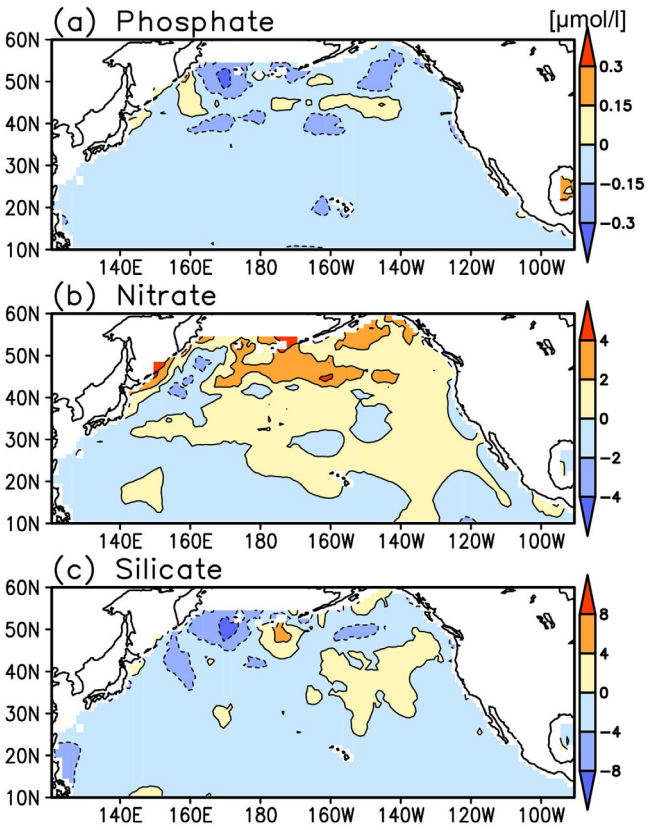

Figure A2. Difference between 10 year annual mean of our estimation and annual mean of WOA13 climatology. (a) Phosphate, (b) nitrate, and (c) silicate.

Our mapping results revealed a characteristic seasonal distribution for each nutrient and can be a useful reference for fixed station and/or line observations. Our basin-wide distribution of drawdown ratios can also be weighed against the distribution of phytoplankton functional type derived from satellite ocean color data [e.g., *Hirata et al.*, 2011].

In terms of global warming, trends of nutrient concentration have been assessed by others without clear patterns emerging except perhaps in the Oyashio region east of Japan [e.g., *Freeland et al.*, 1997; *Ono et al.*, 2002; *Whitney*, 2011]. However, natural variability, such as the PDO, affects the increasing trend especially if the period of analysis is short. Therefore, clarifying of nutrient change associated with climate variability is important to understand the global warming signal in the ocean.

Our estimation is confined to the North Pacific because of the extensive nutrient set collected in this area by the Ships of Opportunity programs of NIES and IOS. Similar coverage of the global ocean may be possible through collaboration and improved data archiving.

Appendix A: Comparison With WOA13

We compared our nutrient maps to WOA climatology, using nutrient analytical means in a 1° × 1° monthly resolution of WOA13 [*Garcia et al.*, 2014]. Spatial distributions of our estimates were generally similar to those of WOA13, but our estimates did not show the unnatural large-scale meander of contours in midlatitudes and local maxima along meridional lines (e.g., silicate along 137°E) which appear in WOA13 inconsistently in time and among nutrient components (Figure A1). These unrealistic and inconsistent meanders and local maxima heavily affected estimates of seasonal decreases and their ratios, and made their spatial characteristics vague (not shown here). Our maps are useful when analyzing small but important temporal variability of biogeochemical conditions for ecosystems such as plankton phenology in wide areas of the North Pacific.

In terms of the box-mean time series, agreement with measurements was better in our estimation than in WOA13 in East Japan areas, especially for summer minima of phosphate and silicate concentrations (Figure 3). Our estimation did not show unnatural summer maxima which WOA13 showed in East Japan area. Furthermore, our estimation also included interannual variability as discussed in section 5.

Systematic biases between our estimates and WOA13 were observed in several regions (Figure A2). Our phosphate and silicate estimates were slightly lower than WOA13 throughout most of the study area, while our nitrate estimate was higher in the subarctic. Those differences were partly from temporal differences between nutrient observations from NIES, IOS, and PACIFICA and those used for calculation of WOA13. Original nutrient data of the PACIFICA database, which include only the data observed after 1990, contained intercruise systematic errors of over 10% before the synthesis [*Suzuki et al.*, 2013]. In the case of older data, which is included in WOA13, larger errors could potentially be found. In addition, longer-term change of

surface nutrient concentration can make systematic bias between databases based on different time window. For example, *Whitney et al*. [2011] showed increasing trend of winter surface nitrate from 1990s to 2000s in the eastern subarctic Pacific. This could explain larger nitrate concentrations in our estimates based on the after-2000 observation data than those of WOA13 in the eastern subarctic.

Acknowledgments
We appreciate Seabord International Shipping Co., Mitsui O.S.K. Lines Co, Toyofuji Shipping Co., and Kagoshima Senpaku Co. for their generous cooperation with the NIES VOS program. We would like to thank the captain, officers, crews, and observers onboard M/S Skaugran, M/S Alligator Hope, M/S Pyxis, and M/S Trans Future 5 for the superb support and collection of water samples. We also thank S. Kariya, T. Yamada, and J. Yamamura of the Global Environmental Forum Foundation, and R. Bellegay and M. Davelaar of Fisheries and Oceans Canada, for their constant assistance with the observations. We acknowledge the assistance of A. Inagaki for data quality analysis of NIES and IOS nutrient data sets, and the inspiration from Y. W. Watanabe. This work was financially supported by the Global Environment Research Account for National Institutes by the Ministry of Environment, and Grant-in-Aid for Scientific Research on Innovative Areas, Japan.

References

Behrenfeld, M. J., and P. G. Falkowski (1997), Photosynthetic rates derived from satellite-based chlorophyll concentration, *Limnol. Oceanogr.*, *42*, 1–20.
Bonjean, F., and G. S. E. Lagerloef (2002), Diagnostic model and analysis of the surface currents in the Tropical Pacific Ocean, *J. Phys. Oceanogr.*, *32*, 2938–2954.
Boyer, T. P., et al. (2013), *World Ocean Database 2013, NOAA Atlas NESDIS 72*, edited by S. Levitus and A. Mishonov, 209 pp. [Available at http://data.nodc.noaa.gov/woa/WOD13/DOC/wod13_intro.pdf.]
Carton, J. A., S. A. Grodsky, and H. Liu (2008), Variability of the oceanic mixed layer, 1960–2004, *J. Clim.*, *21*, 1029–1047, doi:10.1175/2007JCLI1798.1.
Cayan, D. (1992), Latent and sensible heat flux anomalies over the northern oceans: The connection to monthly atmospheric circulation, *J. Clim.*, *5*, 354–369.
Chavez, F. P., S. K. Service, and S. E. Buttrey (1996), Temperature-nitrate relationships in the central and eastern tropical Pacific, *J. Geophys. Res.*, *101*, 20,553–20,563, doi:10.1029/96JC01943.
Deutsch, C., J. L. Sarmiento, D. M. Sigman, N. Gruber, and J. P. Dunne (2007), Spatial coupling of nitrogen inputs and losses in the ocean, *Nature*, *445*, 163–167.
Eppley, R. W., and B. J. Peterson (1979), Particulate organic matter flux and planktonic new production in the deep ocean, *Nature*, *282*, 677–680.
Freeland, H., K. Denman, C. S. Wong, F. Whitney, and R. Jaques (1997), Evidence of change in the mixed layer in the Northeast Pacific Ocean, *Deep Sea Res., Part I*, *44*, 2117–2129.
Garcia, H. E., R. A. Locarnini, T. P. Boyer, J. I. Antonov, O. K. Baranova, M. M. Zweng, J. R. Reagan, and D. R. Johnson (2014), *World Ocean Atlas 2013, Volume 4: Dissolved Inorganic Nutrients (Phosphate, Nitrate, Silicate), NOAA Atlas NESDIS 76*, edited by S. Levitus and A. Mishonov, 25 pp. [Available at http://data.nodc.noaa.gov/woa/WOA13/DOC/woa13_vol4.pdf.]
Garside, C. J., and C. Garside (1995), Euphotic-zone nutrient algorithms for the NABE and EqPac study sites, *Deep Sea Res., Part II*, *42*, 335–342.
Goes, J. I., T. Saino, J. Ishizaka, C. S. Wong, and Y. Nojiri (2000), Estimating sea surface nitrate from space by compound remote sensing, *Geophys. Res. Lett.*, *27*, 1263–1265.
Goes, J. I., K. Sasaoka, H. R. Gomes, S Saitoh, and T. Saino (2004), A comparison of the seasonality and interannual variability of phytoplankton biomass and production in the western and eastern gyres of the subarctic Pacific using multi-sensor satellite data, *J. Oceanogr.*, *60*, 75–91.
Harrison, P. J., F. A. Whitney, A. Tsuda, H. Saito, and K. Tadokoro (2004), Nutrient and plankton dynamics in the NE and NW gyres of the subarctic Pacific Ocean, *J. Oceanogr.*, *60*, 93–117.
Hashihama, F., S. Kinouchi, S. Suwa, M. Suzumura, and J. Kanda (2013), Sensitive determination of enzymatically labile dissolved organic phosphorus and its vertical profiles in the oligotrophic western North Pacific and East China Sea, *J. Oceanogr.*, *69*, 357–367, doi:10.1007/s10872-013-0178-4.
Hirata, T., et al. (2011), Synoptic relationships between surface Chlorophyll-a and diagnostic pigments specific to phytoplankton functional types, *Biogeosciences*, *8*, 311–327, doi:10.5194/bg-8-311-2011.
Honda, M., K. Imai, Y. Nojiri, F. Hoshi, T. Sugawara, and M. Kusakabe (2002), The biological pump in the northwestern North Pacific based on fluxes and major components of particulate matter obtained by sediment-trap experiments (1997–2000), *Deep Sea Res., Part II*, *49*, 5595–5625.
Hosoda, S., T. Ohira, and T. Nakamura (2008), A monthly mean dataset of global oceanic temperature and salinity derived from Argo float observations, *JAMSTEC Rep. Res. Dev.*, *8*, 47–59.
Hosoda, S., T. Ohira, K. Sato, and T. Suga (2010), Improved description of global mixed-layer depth using Argo profiling floats, *J. Oceanogr.*, *66*, 773–787.
Imai, K., Y. Nojiri, N. Tsurushima, and T. Saino (2002), Time series of seasonal variation of primary productivity at station KNOT (44°N, 155°E) in the sub-arctic western North Pacific, *Deep Sea Res., Part II*, *49*, 5395–5408.
Krishnamurthy, A., J. K. Moore, N. Mahowald, C. Luo, and C. S. Zender (2010), Impacts of atmospheric nutrient inputs on marine biogeochemistry, *J. Geophys. Res.*, *115*, G01006, doi:10.1029/2009JG001115.
Lee, K. (2001), Global net community production estimated from the annual cycle of surface water total dissolved inorganic carbon, *Limnol. Oceanogr.*, *46*, 1287–1297.
Lee, K., D. M. Karl, R. Wanninkhof, and J. Z. Zhang (2002), Global estimates of net carbon production in the nitrate-depleted tropical and subtropical oceans, *Geophys. Res. Lett.*, *29*(19), 1907, doi:10.1029/2001GL014198.
Lee, K., L. T. Tong, F. J. Millero, C. L. Sabine, A. G. Dickson, C. Goyet, G.-H. Park, R. Wanninkhof, R. A. Feely, and R. M. Key (2006), Global relationships of total alkalinity with salinity and temperature in surface waters of the world's oceans, *Geophys. Res. Lett.*, *33*, L19605, doi:10.1029/2006GL027207.
Lefèvre, N., A. J. Watson, and A. R. Watson (2005), A comparison of multiple regression and neural network techniques for mapping in situ pCO_2 data, *Tellus, Ser. B*, *57*, 375–384, doi:10.1111/j.1600-0889.2005.00164.x.
Mantua, N. J., S. R. Hare, Y. Zhang, J. M. Wallace, and R. C. Francis (1997), A Pacific interdecadal climate oscillation with impacts on salmon production, *Bull. Am. Meteorol. Soc.*, *78*, 1069–1079.
Martin, J. H., et al. (1994), Testing the iron hypothesis in ecosystems of the equatorial Pacific Ocean, *Nature*, *371*, 123–129, doi:10.1038/371123a0.
Miller, A. J., D. R. Cayan, T. P. Barnett, N. E. Graham, and J. M. Oberhuber (1994), Interdecadal variability of the Pacific Ocean: Model response to observed heat flux and wind stress anomalies, *Clim. Dyn.*, *9*, 287–302.
Miller, A. J., F. Chai, S. Chiba, J. R. Moisan, and D. J. Neilson (2004), Decadal-scale climate and ecosystem interactions in the North Pacific Ocean, *J. Oceanogr.*, *60*, 163–188.

Morel, A., Y. Huot, B. Gentili, P. J. Werdell, S. B. Hooker, and B. A. Franz (2007), Examining the consistency of products derived from various ocean color sensors in open ocean (Case 1) waters in the perspective of a multi-sensor approach, *Remote Sens. Environ.*, *111*, 69–88.

Morel, A., H. Claustre, and B. Gentili (2010), The most oligotrophic subtropical zones of the global ocean: Similarities and differences in terms of chlorophyll and yellow substance, *Biogeosciences*, *7*, 3139–3151, doi:10.5194/bg-7-3139-2010.

Murphy, P. P., Y. Nojiri, Y. Fujinuma, C. S. Wong, J. Zeng, T. Kimoto, and H. Kimoto (2001), Measurements of surface seawater fCO2 from volunteer commercial ships: Techniques and experiences from Skaugran, *J. Atmos. Ocean Technol.*, *18*, 1719–1734.

Nakaoka, S., M. Telszewski, Y. Nojiri, S. Yasunaka, C. Miyazaki, H. Mukai, and N. Usui (2013), Estimating temporal and spatial variation of sea surface pCO_2 in the North Pacific using a self organizing map neural network technique, *Biogeosciences*, *10*, 6093–6106, doi:10.5194/bg-10-6093-2013.

Nishioka, J., et al. (2007), Iron supply to the western subarctic Pacific: Importance of iron export from the Sea of Okhotsk, *J. Geophys. Res.*, *112*, C10012, doi:10.1029/2006JC004055.

Nishioka, J., T. Ono, H. Saito, K. Sakaoka, and T. Yoshimura (2011), Oceanic iron supply mechanisms which support the spring diatom bloom in the Oyashio region, western subarctic Pacific, *J. Geophys. Res.*, *116*, C02021, doi:10.1029/2010JC006321.

Ono, T., K. Tadokoro, T. Midorikawa, J. Nishioka, and T. Saino (2002), Multi-decadal decrease of net community production in western subarctic North Pacific, *Geophys. Res. Lett.*, *29*(8), 1186, doi:10.1029/2001GL014332.

Peña, M. A., and D. E. Varela (2007), Seasonal and interannual variability in phytoplankton and nutrient dynamics along Line P in the NE subarctic Pacific, *Prog. Oceanogr.*, *75*, 200–222.

Polovina, J. J., G. T. Mitchum, and G. T. Evans (1995), Decadal and basin-scale variation in mixed layer depth and the impact on biological production in the central and North Pacific, 1960–1988, *Deep Sea Res., Part I*, *42*, 1701–1716.

Reynolds, R. W., N. A. Rayner, T. M. Smith, D. C. Stokes, and W. Wang (2002), An improved in situ and satellite SST analysis for climate, *J. Clim.*, *15*, 1609–1625.

Saito, H., A. Tsuda, and H. Kasai (2002), Nutrient and plankton dynamics in the Oyashio region of the western subarctic Pacific Ocean, *Deep Sea Res., Part II*, *49*, 5463–5486.

Shiozaki, T., K. Furuya, T. Kodama, S. Kitajima, S. Takeda, T. Takemura, and J. Kanda (2010), New estimation of N_2 fixation in the western and central Pacific Ocean and its marginal seas, *Global Biogeochem. Cycle*, *24*, GB1015, doi:10.1029/2009GB003620.

Signorini, S. R., C. R. McClain, J. R. Christian, and C. S. Wong (2001), Seasonal and interannual variability of phytoplankton, nutrients, TCO2, pCO2, and O2 in the eastern subarctic Pacific (ocean weather station Papa), *J. Geophys. Res.*, *106*, 31,197–31,215, doi:10.1029/2000JC000343.

Steinhoff, T., T. Friedrich, S. E. Hartman, A. Oschlies, D. W. R. Wallace, and A. Körtzinger (2010), Estimating mixed layer nitrate in the North Atlantic Ocean, *Biogeosciences*, *7*, 795–807, doi:10.5194/bg-7-795-2010.

Suzuki, T., et al. (2013), PACIFICA data synthesis project, *ORNL/CDIAC-159, NDP-092*, Carbon Dioxide Inf. Anal. Cent., Oak Ridge Natl. Lab., U.S. Dep. of Energy, Oak Ridge, Tenn.

Sweeney, C., E. Gloor, A. R. Jacobson, R. M. Key, G. McKinley, J. L. Sarmiento, and R. Wanninkhof (2007), Constraining global air-sea gas exchange for CO_2 with recent bomb ^{14}C measurements, *Global Biogeochem. Cycles*, *21*, GB2015, doi:10.1029/2006GB002784.

Takahashi, T., J. Olafsson, J. G. Godard, D. W. Chipman, and S. C. Sutherland (1993), Seasonal variation of CO_2 and nutrient in the high-latitude surface oceans: A comparative study, *Global Biogeochem. Cycles*, *7*, 843–878.

Telszewski, M., et al. (2009), Estimating the monthly pCO_2 distribution in the North Atlantic using a self-organizing neural network, *Biogeosciences*, *6*, 1405–1421, doi:10.5194/bg-6-1405-2009.

Whitney, F. A. (2011), Nutrient variability in the mixed layer of the subarctic Pacific Ocean, 1987–2010, *J. Oceanogr.*, *67*, 481–492.

Whitney, F. A., W. R. Crawford, and P. J. Harrison (2005), Physical processes that enhance nutrient transport and primary productivity in the coastal and open ocean of the subarctic NE Pacific, *Deep Sea Res., Part II*, *52*, 681–706.

Wong, C. S., N. A. D. Waser, Y. Nojiri, F. A. Whitney, J. S. Page, and J. Zeng (2002a), Seasonal cycles of nutrients and dissolved inorganic carbon at high latitudes in the North Pacific Ocean during the Skaugran cruises: Determination of new production and nutrient uptake ratios, *Deep Sea Res., Part II*, *49*, 5317–5338.

Wong, C. S., N. A. D. Waser, Y. Nojiri, W. K. Johnson, F. A. Whitney, J. S. Page, and J. Zeng (2002b), Seasonal and interannual invariability in the distribution of surface nutrients and dissolved inorganic carbon in the northern North Pacific: Influence of El Niño, *J. Oceanogr.*, *58*, 227–243.

Yasunaka, S., Y. Nojiri, S. Nakaoka, T. Ono, H. Mukai, and N. Usui (2013), Monthly maps of sea surface dissolved inorganic carbon in the 695 North Pacific: Basin-wide distribution and seasonal variation, *J. Geophys. Res. Oceans*, *118*, 3843–3850, doi:10.1002/jgrc.20279.

Yasunaka, S., Y. Nojiri, S. Nakaoka, T. Ono, H. Mukai, and N. Usui (2014), North Pacific dissolved inorganic carbon variations related to the Pacific Decadal Oscillation, *Geophys. Res. Lett.*, *41*, 1005–1011, doi:10.1002/2013GL058987.

Zhang, Y., J. M. Wallace, and D. S. Battisti (1997), ENSO-like interdecadal variability: 1900-93, *J. Clim.*, *10*, 1004–1020.